

IDMUNET: A NEW IMAGE DECOMPOSITION INDUCED NETWORK FOR SPARSE FEATURE SEGMENTATION

YUMENG REN, YIMING GAO, CHUNLIN WU*, AND XUE-CHENG TAI

ABSTRACT. UNet and its variants are among the most popular methods for medical image segmentation. Despite their successes in task generality, most of them consider little mathematical modeling behind specific applications. In this paper, we focus on the sparse feature segmentation task and make a task-oriented network design, in which the target objects are sparsely distributed and the background is hard to be mathematically modeled. We start from an image decomposition model with sparsity regularization, and propose a deep unfolding network, namely IDNet, based on an iterative solver, scaled alternating direction method of multipliers (scaled-ADMM). The IDNet splits raw inputs into double feature layers. Then a new task-oriented segmentation network is constructed, dubbed as IDmUNet, based on the proposed IDNets and a mini-UNet. Because of the sparsity prior and deep unfolding method in the structure design, this IDmUNet combines the advantages of mathematical modeling and data-driven approaches. Firstly, our approach has mathematical interpretability and can achieve favorable performance with far fewer learnable parameters. Secondly, our IDmUNet is robust in a simple end-to-end training with explainable behaviors. In the experiments of retinal vessel segmentation (RVS), IDmUNet produces the state-of-the-art results with only 0.07m parameters, whereas SA-UNet, one of the latest variants of UNet, contains 0.54m and the original UNet 31.04m. Moreover, the training procedure of our network converges faster without overfitting phenomenon. This decomposition-based network construction strategy can be generalized to other problems with mathematically clear targets and complicated unclear backgrounds.

1. INTRODUCTION

UNet [43] and its variants are among the mainstream models for medical image segmentation. They are powerful and universal solvers, disengaging people from burdens of accurate modeling with no performance trade-off. But recent

Key words and phrases. Deep unfolding method, Image decomposition, Sparsity, UNet, Variational model.

Y. Ren and C. Wu are with the School of Mathematical Sciences, Nankai University, Tianjin, China (e-mail: tjrym@outlook.com and wucl@nankai.edu.cn). C. Wu is the corresponding author.

Y. Gao is with the College of Science, Nanjing University of Aeronautics and Astronautics, Nanjing, China (e-mail:gaoyiming@nuaa.edu.cn).

X. Tai is with Department of Mathematics, Hong Kong Baptist University, China (e-mail: xuechengtai@hkbu.edu.hk).

studies [22, 61, 62] showed that the original UNet structure, or, in other words, processing images on multiple scale levels through encoder-decoder pairs, require more sophisticated structures to avoid some defects. For example, obvious overfitting phenomenon and generalizing error are discovered in the experiments in [22]. Recent works to tackle these drawbacks can be roughly divided into two categories. One is to focus on redesigning the U-structure, for example, by replacing convolutional blocks with new designs or rearranging connections between encoders and decoders. These changes extend the applicability of methods, but lack interpretability for specified tasks. The other works try to design novel organizations according to task priors, employing multiple UNets or ResNets to build a giant network like RV-GAN [30]. Sub-networks are regarded as black-box processors and linked together to complete complex tasks. These network designs achieve incredible performance but with high computational cost and dependence on complicated training schemes.

In this paper, we focus on segmenting sparse features from images and propose a task-oriented light-weight network with high performance and far fewer learnable parameters than conventional segmentation networks. In this task, with medical vessel segmentation and roadmap extraction as typical examples, the targets are sparsely distributed and the background is difficult to be mathematically modeled.

To incorporate mathematical properties of task priors, we naturally start from a variational image decomposition model with sparse regularizations. Its efficient solver, scaled alternating direction method of multipliers (scaled-ADMM), is derived and unfolded into an image decomposition network (IDNet), which is different from existing unfolding networks based on reconstruction models. In IDNet, the sparse regularization is kept in the network structure; while the regularization kernels for the background are relaxed to be learned, because of the difficulty of accurate mathematical modeling for the background. We also relax the model and algorithm parameters as learnable ones. This IDNet extracts two feature layers from the input image: the sparse targets layer and the background layer. Based on feature layers extracted, we introduce a mini-UNet, a shallow version of UNet for segmentation. Although containing only few parameters, the mini-UNet suffices to produce favorable results over features extracted by IDNets. We name the architecture with two cascading stages, IDNets and the mini-UNet, as IDmUNet. Through the introduction of sparse regularization and the unfolding methods, IDmUNet combines the advantages of both mathematical modeling and data-driven approaches, and has the following benefits:

- (1) The IDmUNet is mathematically interpretable and can work quite well with far fewer learnable parameters. When applied to the RVS datasets, our IDmUNet can achieve the state-of-the-art performance with only 0.07m parameters, whereas SA-UNet (a latest variant of UNet) contains 0.54m and the original UNet 31.04m.

- (2) Our method is of robust design with a simple end-to-end training. The training procedure of our network model converges faster without overfitting phenomenon. Experimental behaviors of our IDmUNet are highly explainable compared with many pure DNN approaches of black-box nature. The intermediate data, outputs of IDNets, will assist specialists for further analysis, for fields requiring strong confidence like medical imaging.

Our decomposition-based network construction strategy can be easily generalized to a wide range of problems, in which the targets are well-characterized by mathematical priors, while the backgrounds need learnable architectures to fit.

The remainder of this paper is organized as follows. Section 2 describes some related works in detail. In Section 3, we first present the variational model and its scaled-ADMM solver, and then unfold the solver into a network design. The network for sparse feature segmentation is constructed in section 4. Section 5 exhibits training details. Evaluation metrics, datasets and comparisons are given in Section 6. Conclusions and future works are discussed in Section 7.

2. RELATED WORKS

We will review related works on medical image segmentation methods based on UNets, deep unfolding methods and the variational framework for image decomposition.

2.1. UNet Related Medical Image Segmentation Methods. Since [43], UNets and its variants have been widely studied and produce striking results in medical image segmentation. Generally, the UNet structure can be considered as encoder-decoder architectures. State-of-the-art networks further develop the prototype to avoid obvious defects like overfitting phenomenon and achieve higher performance. Most of studies tend to generalize the UNet structure to cover more tasks with self-adaptive feature extraction architectures (and possibly more hyperparameters). They inject new blocks and rearrange the connections. For instance, nested skip-connections [28, 62] were proposed to mitigate the unknown network depth with an efficient ensemble of U-Nets of varying depths. Also, some researchers introduced novel blocks, such as context extractor [21], dual-encoding [49], task consistency learning block [25] and attention mechanisms [22, 59], to name a few. While keeping almost the same scale of learnable parameters with original UNet, they successfully pursued the task-generalality, but usually considered little on task priors.

Meanwhile, others considered task priors and employed multiple UNets (and possibly the other pre-defined networks like ResNets) to construct task-oriented giant networks [30, 37, 54, 61]. Some studies also designed structures served as automatic data-augmentation corresponding to image priors, or in other words, generating pseudo-samples; See [30, 37, 61] and the references therein. With huge

number of learnable parameters, they achieved incredible performance improvement, but lacked interpretability and relied on tricky training procedures with more hyper-parameters, because of the black-box nature without mathematical modeling.

In above methods, [21, 22, 30, 37, 59, 61] consider the vessel segmentation, which relate closely to our work.

2.2. Deep Unfolding Methods. Recently, deep unfolding methods provide essential tools for the network design on problems equipped with clear physical or mathematical models. The implicit layer-like structures in iterative solvers are discovered and further mapped into deep architectures. Model and algorithm parameters are relaxed to be learned from data. In [20], Yann LeCunn first proposed a Learnable-ISTA (LISTA) model inspired by the classical ISTA algorithm, that, as a learnable version, can achieve higher convergence rate. The first n steps of iterative solver are mapped as a n -layer deep network. In [27, 45, 48], iterative solvers for conditional random field(CRF) were unfolded as deep architectures. Later, Yang et al. in [56, 57] unfolded the ADMM algorithm solving the compressive sensing model into a network, achieving high performance with less computational cost. For reconstruction problems, the primal-dual network was proposed in [1] with applications in CT and MRI reconstruction. Note that these methods are different from ours, which starts from a variational decomposition model.

To understand the dynamic systems interpretation of ResNet [14], the prediction models like time-dependent PDEs [39, 40] and ODEs [10, 17, 26, 51] were also categorized in unfolding networks. For instance, in [39], the forward Euler scheme was considered as the temporal discretization of the evolution PDE and resulted in iterative algorithms. Moreover, there were also networks with explicit depth [17, 26], for which alternative back-propagation procedures based on ODE-theory were proposed, instead of the chain rule.

2.3. Variational Framework For Image Decomposition. In mathematical image processing community, one important task is to decompose one single image into two or more useful components. These components illustrate different image structures and benefit many high-level vision tasks [2, 31, 36].

In variational framework, the related minimization model should thus consist of two or more regularizers for different components and dates back to infimal convolution techniques [8]. Following [8], people considered various decomposition models. Usually there is one cartoon component regularized by the TV (total variation) prior [8, 46] or non-convex TV prior [9, 13, 23]. The TV prior is a composition of ℓ_1 -norm and gradient operators, characterizing the sparsity [7, 11, 12] of an image in gradient domain. The other components depend on applications, such as cartoon-texture decomposition [24, 29, 44], Retinex illumination estimation [33, 38, 41, 42] and intensity inhomogeneity removal [4, 5, 9, 23]. Also, in [4, 5, 9, 23] two-stage

methods were proposed to complete segmentation task. We note that these are not data-driven methods and need to select parameters manually.

3. IMAGE DECOMPOSITION NETWORK

In this section, we focus on building an image decomposition network to extract two feature layers with a sparse one, following the idea of deep unfolding. We first introduce a variational model with two regularization terms. This double-feature decomposition model belongs to the family of inf-convolution type models [8], for which various splitting algorithms [19] can be employed efficiently, with convergence guarantee. Following the idea of deep unfolding [1, 20, 56, 57], we construct the image decomposition network (IDNet) over the optimization solver.

3.1. Variational Model. We first give basic notations to construct our models. Without loss of generality, the 2D gray image u can be represented as an $N \times N$ array. We denote $X = \mathbb{R}^{N \times N}$ and equip X with inner product $\langle \cdot, \cdot \rangle$ and $\| \cdot \|$ as follows: For $u, v \in X$, $\langle u, v \rangle = \sum_{i=1}^N \sum_{j=1}^N u_{i,j} v_{i,j}$, $\|u\|_2 = \sqrt{\langle u, u \rangle}$, $\|u\|_1 = \sum_{i=1}^N \sum_{j=1}^N |u_{i,j}|$. For more notations like ∇_x and ∇_y , one can refer to [52].

For a gray-scale image $f \in X$, we introduce a variational model to decompose it into two feature layers: one is a sparse target layer $v \in X$, the other is a background layer $u \in X$. According to [7, 11, 12], we use ℓ_1 norm to characterize the sparse layer v . The complicated background layer u is, however, assumed to be characterized by the sparsity in the domain of a group of convolution kernels, which are data-dependent. Our decomposition model is then given as follows:

$$(1) \quad \min_{u,v \in X} \beta \|v\|_1 + \sum_{m=1}^M \alpha_m \|K_m u\|_1 + \frac{1}{2} \|u + v - f\|_2^2,$$

where each $K_m : X \rightarrow X$ is a 2D-convolutional operator and $\alpha_m > 0$, $\beta > 0$ are some regularization parameters, with $m = 1, 2, \dots, M$. A special case of this model is to set $M = 2$ and (K_1, K_2) as the 2D-gradient operator, and reads

$$(2) \quad \min_{u,v} \beta \|v\|_1 + \alpha_1 \|\nabla_x u\|_1 + \alpha_2 \|\nabla_y u\|_1 + \frac{1}{2} \|u + v - f\|_2^2.$$

We mention that an isotropic variant of model (2) was proposed in [6] for mixed noise removal, in a non- data driven fashion. Very recently we got aware [32] using a similiar model for structure-texture decomposition, but with only two terms, which is essentially an implusive noise removal model. Instead of constructing an unrolling network structure suitable for end-to-end training, they embedded a pre-trained CAN [58] network into their iterative algorithm, following the plug-and-play idea.

3.2. Iterative Solver. The model (1) is, although non-smooth, but convex and with separable structures. It can be efficiently solved by various splitting methods with convergence guarantee [19], such as ADMM, primal-dual methods and split Bregman iteration. In this paper, we take the scaled-ADMM [3, 18]. The algorithm uses variable splitting and the augmented Lagrangian function, which can alternatively solve some simple subproblems.

We first introduce auxiliary variables $q \in X$ and $p = (p_1, p_2, \dots, p_M) \in X^M = \underbrace{X \times X \cdots \times X}_M$, and write the model (1) as the following equivalent one

$$(3) \quad \begin{cases} \min_{\substack{u, v, q \in X \\ p \in X^M}} \beta \|q\|_1 + \sum_{m=1}^M \alpha_m \|p_m\|_1 + \frac{1}{2} \|u + v - f\|_2^2, \\ \text{s.t. } p_m = K_m u, \quad m = 1, 2, \dots, M, \\ q = v. \end{cases}$$

We define its augmented Lagrangian function as

$$(4) \quad \begin{aligned} \mathcal{L}(u, v, p, q; \lambda, \mu) &= \beta \|q\|_1 + \langle \mu, v - q \rangle + \frac{r_q}{2} \|v - q\|_2^2 \\ &+ \sum_{m=1}^M \alpha_m \|p_m\|_1 + \langle \lambda_m, K_m u - p_m \rangle + \frac{r_p}{2} \|K_m u - p_m\|_2^2 \\ &+ \frac{1}{2} \|u + v - f\|_2^2, \end{aligned}$$

with Lagrangian multipliers $\lambda = \{\lambda_m\}$, μ and penalty parameters $r_p > 0, r_q > 0$, which can be reformulated to be

$$(5) \quad \begin{aligned} \widehat{\mathcal{L}}(u, v, p, q; \widehat{\lambda}, \widehat{\mu}) &= \beta \|q\|_1 + \frac{r_q}{2} \|v - q + \widehat{\mu}\|_2^2 - \frac{r_q}{2} \|\widehat{\mu}\|_2^2 \\ &+ \sum_{m=1}^M \alpha_m \|p_m\|_1 + \frac{r_p}{2} \|K_m u - p_m + \widehat{\lambda}_m\|_2^2 - \frac{r_p}{2} \|\widehat{\lambda}_m\|_2^2 \\ &+ \frac{1}{2} \|u + v - f\|_2^2, \end{aligned}$$

by letting $\widehat{\lambda}_m = \lambda_m / r_p, \widehat{\mu} = \mu / r_q$ as in [3, 18]. We then amount to solve the saddle point problem below:

$$(6) \quad \begin{aligned} &\text{Find } (u^*, v^*, p^*, q^*; \widehat{\lambda}^*, \widehat{\mu}^*) \in X \times X \times X^M \times X \times X^M, \\ &\text{s.t. } \widehat{\mathcal{L}}(u^*, v^*, p^*, q^*; \widehat{\lambda}, \widehat{\mu}) \leq \widehat{\mathcal{L}}(u^*, v^*, p^*, q^*; \widehat{\lambda}^*, \widehat{\mu}^*) \\ &\leq \widehat{\mathcal{L}}(u, v, p, q; \widehat{\lambda}^*, \widehat{\mu}^*), \end{aligned}$$

for all $(u, v, p, q; \widehat{\lambda}, \widehat{\mu}) \in X \times X \times X^M \times X \times X^M$. The scaled-ADMM solver is then presented in Algorithm 1:

Algorithm 1. Scaled-ADMM solver for Saddle Point Problem

1. **Initialization:** $p^{(0)}, q^{(0)}, u^{(0)}, v^{(0)}, \widehat{\lambda}^{(0)}, \widehat{\mu}^{(0)} = 0$

2. **For** $l = 0, 1, \dots$, until convergence:

 Compute $(u^{(l+1)}, v^{(l+1)})$ from

$$(7) \quad \min_{(u,v) \in X \times X} \widehat{\mathcal{L}}(u, v, p^{(l)}, q^{(l)}; \widehat{\lambda}^{(l)}, \widehat{\mu}^{(l)});$$

 Compute $(p^{(l+1)}, q^{(l+1)})$ from

$$(8) \quad \min_{(p,q) \in X^M \times X} \widehat{\mathcal{L}}(u^{(l+1)}, v^{(l+1)}, p, q; \widehat{\lambda}^{(l)}, \widehat{\mu}^{(l)});$$

 Update

$$(9) \quad \begin{cases} \widehat{\lambda}_m^{(l+1)} = \widehat{\lambda}_m^{(l)} + K_m u^{(l+1)} - p_m^{(l+1)}, \\ \widehat{\mu}^{(l+1)} = \widehat{\mu}^{(l)} + v^{(l+1)} - q^{(l+1)}, \end{cases}$$

 where $m = 1, 2, \dots, M$.

Note that each subproblem has an explicit solution or can be solved simply. In (7), computing $(u^{(l+1)}, v^{(l+1)})$ is equivalent to solve a linear system:

$$(10) \quad \begin{pmatrix} E_1 & I \\ I & E_2 \end{pmatrix} \begin{pmatrix} u \\ v \end{pmatrix} = \begin{pmatrix} f + \sum_{m=1}^M r_p K_m^T (p_m^{(l)} - \widehat{\lambda}_m^{(l)}) \\ f + r_q (q^{(l)} - \widehat{\mu}^{(l)}) \end{pmatrix},$$

where I represents the identity operator and

$$(11) \quad \begin{cases} E_1 = \sum_{m=1}^M r_p K_m^T K_m + I, \\ E_2 = r_q I, \end{cases}$$

with K_m^T , the adjoint operator of K_m . For the convolutional operator K_m with periodic boundary condition, (7) can be efficiently solved by FFT [50, 52, 57].

As for (8), we compute $(p^{(l+1)}, q^{(l+1)})$ by

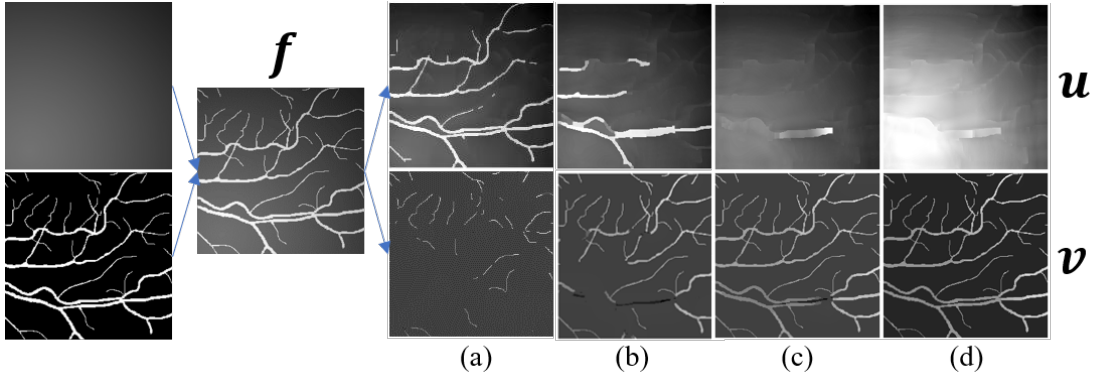


FIGURE 1. Decomposition results (u, v) of a synthetic image by model (1) ($M = 2$ and kernels $K_1 = \nabla_x, K_2 = \nabla_y$) with changing parameters, $(\alpha_1, \alpha_2, \beta)$: $(0.3, 0.3, 0.25)$ in (a), $(0.5, 0.5, 0.15)$ in (b), $(0.58, 0.58, 0.11)$ in (c) and $(0.6, 0.6, 0.1)$ in (d).

$$(12) \quad \begin{cases} p_m^{(l+1)} = \mathcal{S}(K_m u^{(l+1)} + \widehat{\lambda}_m^{(l)}; \alpha_m/r_p), \\ q^{(l+1)} = \mathcal{S}(v^{(l+1)} + \widehat{\mu}^{(l)}; \beta/r_q), \end{cases}$$

where $m \in \{1, 2, \dots, M\}$. \mathcal{S} represents the soft-thresholding operator. In particular, for $x \in \mathbb{R}$ and $\gamma \in \mathbb{R}_+$, $\mathcal{S}(x; \gamma) : \mathbb{R} \rightarrow \mathbb{R}$ is defined as

$$(13) \quad \mathcal{S}(x; \gamma) = \begin{cases} \text{sgn}(x)(|x| - \gamma), & \text{if } |x| \leq \gamma, \\ 0, & \text{else.} \end{cases}$$

Fig. 1 shows a simple synthetic example applying the model (1) and Algorithm 1, with $L = 100$, $M = 2$, $r_p = r_q = 0.07$, kernels $K_1 = \nabla_x, K_2 = \nabla_y$ and different $\alpha_1, \alpha_2, \beta$. With a proper selection of parameters, one can see that the model fulfills the purpose of sparse feature extraction quite well on a synthetic image with simple background. However, the decomposition results depend heavily on the selection. To produce proper results for further processing, we need to carefully choose all these parameters and the iteration number. On the other hand, the background in practice is far more complicated and can not be characterized properly by manually selected kernels. Naturally, we wish to derive a data-driven approach to extract proper features from data via automatically adapting parameters by training. Next, we propose the IDNet, a trainable feature extraction network.

3.3. IDNet. In this section, the IDNet, a trainable feature extractor, is constructed from Algorithm 1 for model (1), following unfolding methods [1, 20, 56, 57]. We mention that these existing literatures all start from reconstruction models and

their constructed networks are for image restoration problems. Here our IDNet is designed based on a variational decomposition model with two feature layers as outputs. The naming of ‘‘IDNet’’ emphasizes this difference between ours and the reconstruction model-based literatures, to show the special objective of our variational model (1). We fix the first L iterations and map each iteration into one network layer. The operators are generalized to network blocks by relaxing the parameters to be learnable, yielding the linear-system solver (LSS) block and the auxiliary-variable-and-multiplier updater (AVMU) block.

Fig. 2a shows the IDNet structure. In Fig. 2a, the network input is f . We set the initial values $(p^{(0)}, q^{(0)}, \widehat{\lambda}^{(0)}, \widehat{\mu}^{(0)}) = 0$ in the first layer. The network state for l -th layer ($l = 0, 1, \dots, L - 1$) is defined as $(p^{(l+1)}, q^{(l+1)}, \widehat{\lambda}^{(l+1)}, \widehat{\mu}^{(l+1)})$, and $(u^{(l+1)}, v^{(l+1)})$ are not passed to the next layer. Please notice that the outputs of the last layer are (u^L, v^L) . We describe more details about these two blocks and their parameters.

3.3.1. LSS Block. The LSS block outputs two images u, v decomposed from f , similar to the operations of (10). Given $p^{(l)}, q^{(l)}, \widehat{\mu}^{(l)}$ and $\widehat{\lambda}^{(l)}$, the outputs of this block, $LSS^{(l)}$, are defined as

$$(14) \quad u^{(l+1)} = (E_2 E_1^{(l)} - I)^{-1} (E_2 b_1^{(l)} - b_2^{(l)}),$$

$$(15) \quad v^{(l+1)} = -E_1^{(l)} u^{(l+1)} + b_1^{(l)},$$

where I is the identity matrix in $\mathbb{R}^{N^2 \times N^2}$ and

$$(16) \quad \begin{cases} E_1^{(l)} = \sum_{m=1}^M r_p K_m^{(l)T} K_m^{(l)} + I, \\ E_2 = r_q I, \\ b_1^{(l)} = f + \sum_{m=1}^M r_p K_m^{(l)T} (p_m^{(l)} - \widehat{\lambda}_m^{(l)}), \\ b_2^{(l)} = f + r_q (q^{(l)} - \widehat{\mu}^{(l)}). \end{cases}$$

Notice that we relax K_m in Algorithm 1 to be $K_m^{(l)}$, in order to increase the network capacity. Compared to (11), $K_m^{(l)}$ and $E_1^{(l)}$ are not shared between layers.

3.3.2. AVMU Block. The AVMU block updates the auxiliary variables and multipliers according to u and v , respectively. Notice that $(p^{(l+1)}, \widehat{\lambda}^{(l+1)})$ and $(q^{(l+1)}, \widehat{\mu}^{(l+1)})$ in (12) can be computed in parallel, so we define two parallel blocks with similar structures. Given $(u^{(l+1)}, v^{(l+1)})$ and $(p^{(l)}, \widehat{\lambda}^{(l)})$, the computational sequence of

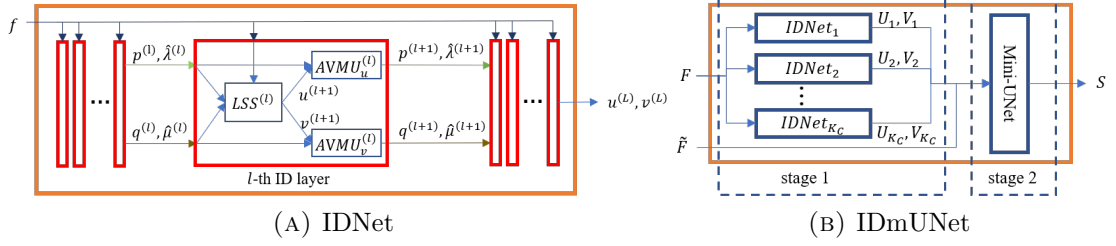


FIGURE 2. The structure of the IDNet and IDmUNet

AVMU $_u$ is defined as

$$(17) \quad \begin{cases} e_m^{(l)} = K_m^{(l)} u^{(l+1)}, \\ p_m^{(l+1)} = \mathcal{S}(e_m^{(l)} + \hat{\lambda}_m^{(l)}; \alpha_m^{(l)}/r_p), \\ \hat{\lambda}_m^{(l+1)} = \hat{\lambda}_m^{(l)} + e_m^{(l)} - p_m^{(l+1)}, \end{cases}$$

where $m = 1, 2, \dots, M$. Given $(u^{(l+1)}, v^{(l+1)})$ and $(q^{(l)}, \hat{\mu}^{(l)})$, the computational sequence of AVMU $_v$ is defined as

$$(18) \quad \begin{cases} e^{(l)} = v^{(l+1)}, \\ q^{(l+1)} = \mathcal{S}(e^{(l)} + \hat{\mu}^{(l)}; \beta^{(l)}/r_q), \\ \hat{\mu}^{(l+1)} = \hat{\mu}^{(l)} + e^{(l)} - q^{(l+1)}. \end{cases}$$

We note that parameters $\alpha_m^{(l)}$ and $\beta^{(l)}$ relaxed from (12) are not shared between each layer.

3.3.3. Network Parameters. These blocks are organized as Fig. 2a. In IDNet, we aim to learn the following parameters: r_p, r_q shared for all layers, $K_m^{(l)}$ in LSS block and $\alpha^{(l)}, \beta^{(l)}$ in AVMU block, where $m \in \{1, 2, \dots, M\}$ and $l \in \{0, 1, \dots, L-1\}$. Calculations in IDNet are basic, including element-wise non-linear functions, arithmetics of matrices and 2D-convolutions, just like those in a typical CNN. Therefore, the back-propagation can be conducted by the autograd package of deep-learning framework like PyTorch.

4. IDMUNET

In this section, we propose our sparse feature segmentation network, IDmUNet, in which the target objects are sparsely distributed across the complicated background. In Fig. 2b, our IDmUNet consists of two cascading stages: the first one employs a group of IDNets to extract meaningful feature layers and the second one uses a mini-UNet to operate segmentation on them. We mention that this structure is inspired by recent variational two-stage segmentation methods [4, 5, 9, 23]. Our variational model in this papers is different from theirs. Notice that we use a group

of IDNets with shared parameters in the first stage, so learnable parameters in IDmUNet consist of only one copy of parameters in the IDNet along with those in the mini-UNet. There have been many works that injected different feature-extraction blocks into the UNet structure like [21, 60], but as far as we know, our IDmUNet is the first one to integrate image decomposition induced feature-extraction blocks into the UNet, following the idea of deep unfolding and variational models.

In the first stage of IDmUNet, the IDNet, trainable feature-extracting block introduced in Section 3.3, decomposes a single-channeled input f into a pair of feature layers (u, v) . The deep unfolding procedure ensures that the parameters in IDNet could be initialized by the corresponding values of its backbone, the scaled-ADMM solver in Algorithm 1. Furthermore, the layer-like structures of IDNet allow us to implement an efficient back-propagation procedure and integrate it as sub-network into classical DNN architectures.

In the second stage, we take a mini-UNet, a shallow version of UNet, as the universal clustering block, for its capability of segmentation on various types of inputs. It acts on the multi-channel feature layers produced by the first stage. If we individually use such a mini-UNet for segmentation, it usually behaves worse than a full-sized UNet. However, based on the extracted features of our IDNets, it can work quit well. The ablation experiments in Section 6.4 show that mini-UNet acts quite well on the feature layers produced by the first stage and our light-weight IDmUNet outperforms the original full-sized UNet.

We note that, in practice, the samples from dataset are multi-channel and not all the channels need to be decomposed. So, in Fig. 2b, we denote those to be processed by the IDNets with shared parameters as a multi-channel image F , and the rest of them as \tilde{F} . The number of IDNet is denoted as K_C . Each channel F_k of F will be processed by an IDNet. The decomposition result is denoted as (U_k, V_k) , where $k = 1, 2, \dots, K_C$. Then, $U = \{U_k\}_{k=1}^{K_C}$, $V = \{V_k\}_{k=1}^{K_C}$ and \tilde{F} are stacked as a multi-channel image for the following mini-UNet. S in Fig. 2b represents the segmentation result.

5. TRAINING

In this section, we describe the loss function, the structural parameters of IDmUNet and the configurations of training procedure.

5.1. Loss Function. We focus on binary segmentation task in this paper. Each ground-truth is a binary-valued mask, so we take cross-entropy as the loss function:

$$(19) \quad \text{loss} = \frac{1}{|\Gamma|} \sum_{x \in \Gamma} (-T(x) \log P(x) - (1 - T(x)) \log(1 - P(x))),$$

where Γ represents all pixels of the input image, $P(x) \in [0, 1]$ is the prediction of IDmUNet at pixel x , and $T(x)$ is the ground-truth label at pixel x with $T(x) = 1$ for labeled x or $T(x) = 0$.

5.2. Structural Parameters of IDmUNet. For IDNet, we set the width of ID-layer as $M = 4$ and the depth as $L = 16$. The size of convolution kernels in each ID-layer is set to $(2R + 1) \times (2R + 1)$ and $R = 2$. The mini-UNet we used is a very shallow UNet with only 16 start-channels and 13 convolutional layers. Moreover, the bilinear option provided by PyTorch framework, is enabled in up-sampling operations of mini-UNet, and each ReLU activation unit is followed by a layer of batch normalization to accelerate network convergence. The parameters of mini-UNet contains 66k parameters, which is nearly 450 times smaller than a full-sized UNet(64 start-channels and 23 convolutional layers). We take the IDmUNet with such settings as our candidate in experiments, except for those in Section 6.5.

5.3. Training Configurations. We divide learnable parameters of IDmUNet into two groups and train them with different learning rates, D-group for the parameters of IDNet and U-group for those of mini-UNet. A basic end-to-end training suffices to achieve good results for our IDmUNet. The training procedure contains 4 phases. The learning rate of each phase starts from the value given in Table 1. They will be controlled by scheduler provided by deep learning framework.

TABLE 1. Configurations of training phases

Phase	Learning rate		Epoches
	D-group	U-group	
1	0	0.02	20
2	0.0025	0.01	25
3	0.001	0.01	50
4	0.0005	0.005	50

6. EXPERIMENTS ON RETINAL VESSEL SEGMENTATION

In this section, we apply our IDmUNet on RVS tasks. We first describe how to prepare data and initialize network parameters. Then the performances of IDmUNet with experiments on different purposes are verified. Under the implementation framework of PyTorch, all experiments are conducted on a desktop with one GPU device, RTX 2080Ti 11G. We use the SGD optimizer and ReduceLROnPlateau scheduler for the training procedure.

6.1. Data Preparation. In this subsection, we first introduce RVS datasets for experiments, then describe details about data transformations. Since our IDNet is designed for additive features separation, we should apply proper data transformation to the physical imaging procedures that not fit the additive relationship.

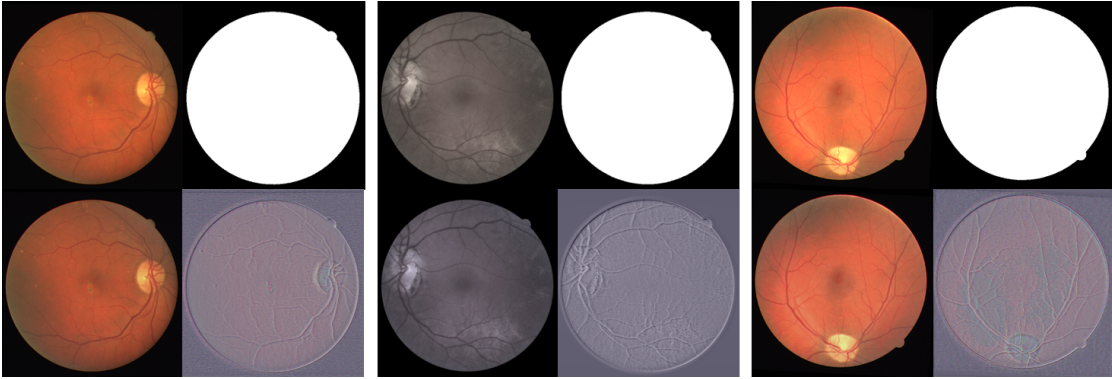


FIGURE 3. Example images from inputs and outputs of trained ID-Nets for augmented DRIVE dataset. In each image group, the first row contains fundus image \mathcal{F} and FOV, and the second row contains feature layers \mathcal{U}, \mathcal{V} .

Here we take the most widely used DRIVE [47] dataset, as well as another dataset CHASE_DB1 [16] with larger image samples, for RVS tasks. They have very few samples, 20+20 (train+test) for DRIVE and 20+8 for CHASE_DB1. The fundus images from DRIVE with the size of 565×584 and those from CHASE_DB1 with the size of 999×960 pixels are online-cropped to 320×320 randomly for each training epoch. For DRIVE and CHASE_DB1, FOV (Field of view) is produced by datasets, served as the input \tilde{F} for IDmUNet in Fig. 2b. For convenience of training and doing comparisons, we use the pre-augmented version of these two datasets used in [22], with 234 samples.

Fundus images [15] from RVS datasets are optical photos, feature layers in which satisfy the multiplicative relationship formulated by the Retinex theory [35, 55]. Consequently, we represent each image as the product of the target feature layer and the background feature layer. Through logarithmic transformation, the flow forms of data in our network are given as below: For $\mathcal{F} = \{\mathcal{F}_k\}_{k=1}^{K_C}$, $K_C = 3$, a fundus RGB-image to be decomposed,

$$\begin{cases} f_k = \log \mathcal{F}_k, \\ (u_k, v_k) = \text{IDNet}_k(f_k), \\ (\mathcal{U}_k, \mathcal{V}_k) = (\exp u_k, \exp v_k), \end{cases}$$

where $k = 1, 2, \dots, K_C$. $\mathcal{U} = \{\mathcal{U}_k\}$, $\mathcal{V} = \{\mathcal{V}_k\}$ and \tilde{F} are further stacked as a multi-channel image entering the mini-UNet, where the field of view (FOV) [15] from RVS datasets usually serves as \tilde{F} . Finally, we have a 7-channel image as the input of mini-UNet. Notice that, in practice, the IDNets we used in the first stage share one copy of parameters. Examples of the inputs from augmented DRIVE

dataset as well as the outputs from IDNets in a trained IDmUNet (Section 6.6) are shown in Fig. 3.

6.2. Learnable Parameters Initialization. The learnable parameters in an L -layer IDmUNet can be divided into three categories: regularization kernels $\{K_m^{(l)}\}_{m=1}^M$, model parameters $\{\alpha_m^{(l)}\}_{m=1}^M$, $\beta^{(l)}$ and algorithm parameters r_p , r_q , where $l = 0, 1, \dots, L - 1$. Notice that there are no learnable parameters for the sparsity regularization, because such kind of regularization has accurate mathematical modeling and the sparsity property is obvious for vessels, for the fact that in the test set Y of DRIVE dataset, 556,532 pixels are marked as vessel and 3,981,611 as background (12.3% vessel) [15].

The regularization kernels $\{K_m^{(l)} | m = 1, 2, \dots, M, l = 0, 1, \dots, L - 1\}$ are initialized as the 2D forward difference operators with periodic boundary condition [52], inspired by Retinex decomposition operators in [33, 42, 52]. For M is even, we set $K_{2s-1}^{(l)} = \nabla_x$ and $K_{2s}^{(l)} = \nabla_y$, where $s = 1, 2, \dots, M$ and $l = 0, 1, \dots, L - 1$.

Initial values for model parameters and algorithm parameters are selected manually from pre-experiments in Algorithm 1. We set algorithm parameters $r_p = r_q = 0.07$ and model parameters $\alpha_m^{(l)} = 1.5/M$, $\beta^{(l)} = 0.07$, with $m = 1, 2, \dots, M$, $l = 0, 1, \dots, L - 1$. We mention that this kind of initialization is nearly the same as the settings in the example of Fig. 1.

6.3. Evaluation Metrics. As in the literature, the performance of segmentation is evaluated mainly by the AUC (area under the ROC curve) score. It is a widely used measurement for segmentation and classification tasks in deep learning. If the AUC value is 1, it means perfect segmentation. We also compute scores of ACC, and MCC to enlarge the scope of comparison. All these scores are based on pixel-wise comparisons between the segmentation results with the corresponding ground truth. The results of each pixel comparison are divided into true positive (TP), false positive (FP), false negative (FN), and true negative (TN). Details of these measurements can be found in [15]. If not specified, we calculate all these scores on the test sets and take the average value.

6.4. Ablation Experiments. We conduct experiments between the full-sized UNet [43], the mini-UNet in Section 4 and our IDmUNet on DRIVE and CHASE_DB1 datasets. Fig. 4 and Table 2 give details about the comparison. As ones can see, the IDmUNet achieves the highest accuracy and behaves the most stable in the training procedure. It has far less learnable parameters than a full-sized UNet.

Due to the good feature extraction ability of IDNets, our IDmUNet achieves good performance, although its parameter scale is nearly 1/450 of the full-sized UNet. Table 2 shows the amount of learnable parameters involved in the three networks as well as the U-structure shape appeared in each network structure.

Fig. 4 shows the change of average AUC during the training procedure measured on the test datasets. We can see that IDmUNet has an obvious improvement

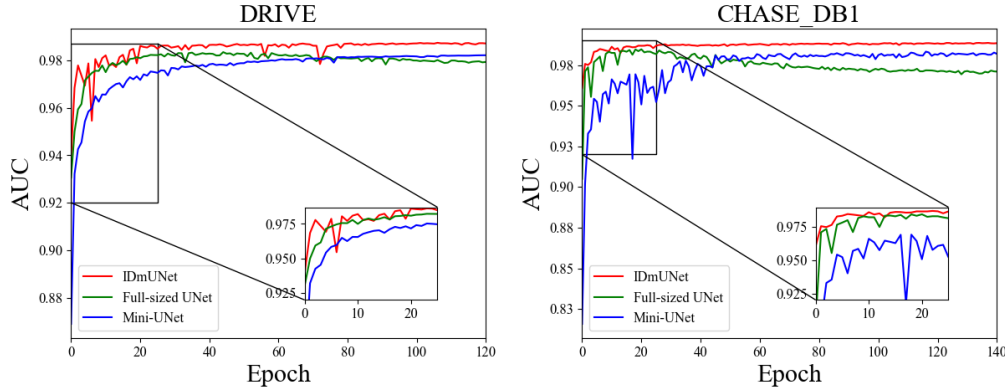


FIGURE 4. Compararions about average-AUC score versus epoch in two datasets during training procedure in ablation experiments (Section 6.4).

TABLE 2. Comparisons about parameter scale and performance between single-UNet-based neural network methods on DRIVE and CHASE_DB1 datasets

Networks	Year	U-structure shape		Parameter number*		DRIVE			CHASE_DB1		
		Depth**	Start channel	Abs.	Rel.	AUC	ACC	MCC	AUC	ACC	MCC
IDmUNet(Ours)	-	2	16	0.070e6	1.00	0.9874	0.9699	0.8058	0.9882	0.9755	0.7859
mini-UNet	-	2	16	0.066e6	0.94	0.9840	0.9611	0.7873	0.9832	0.9726	0.7621
SAUNet [22]	2021	3	16	0.54e6	7.74	0.9864	0.9698	0.8097	0.9905	0.9755	0.8097
StudyGroup [61]**	2021	-	-	15.53e6	223.27	0.9887	0.9703	-	0.9920	0.9771	-
AGNet [59]	2019	4	32	9.34e6	134.19	0.9856	0.9692	-	0.9863	0.9743	-
Vessel-Net [53]	2019	2	32	0.59e6	8.42	0.9821	0.9578	-	0.9860	0.9661	-
M2U-Net [34]	2019	2	32	0.55e6	7.90	0.9714	0.9630	-	0.9666	0.9703	-
UNet [43]	2015	4	64	31.04e6	446.22	0.9789	0.9666	0.7839	0.9838	0.9733	0.7733

* The digits in column Abs. is measured by functions provided by deep learning framework.

** Depth means the number of down-/up- sampling pairs.

*** StudyGroup method using K-fold cross-validation procedure for generating pseudo-samples. Its stack multiple UNet in its model, the structure of model and the motivation of the method are quite different to other methods here. We mention it only for the completeness of the discussion.

on the accuracy of segmentation, compared to the mini-UNet. Also, overfitting phenomenon is only discovered on the full-sized UNet. The AUC score of the full-sized UNet has a decline trend after 40 epoches on DRIVE and 20 epoches on CHASE_DB1. IDmUNet behaves stable with quickly increased AUC score during the whole training procedure.

6.5. The influence of the structural parameters of IDNets. Since there are many studies on the influence of UNet’s structural parameters, we here focus on the IDNet proposed in this paper. In particular, we exhibit experiments to

TABLE 3. Experiments on the influence of structural parameters M and R in terms of AUC, with $L = 12$

	$R = 2$			$M = 2$		
	$M=2$	$M=4$	$M=6$	$R=1$	$R=2$	$R=3$
AUC	0.9869	0.9871	0.9871	0.9870	0.9871	0.9871

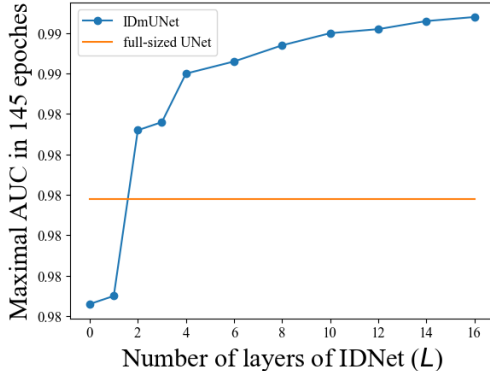


FIGURE 5. Experiments on the influence of structural parameter L in terms of AUC, with $M = 4, R = 2$

discover how structural parameters influence the performance of IDmUNet, such as the width M of an ID-layer (the number of convolutional kernels), the depth L of an IDNet, and the size R of convolutional kernels. We take the IDmUNet ($M = 4, L = 12, R = 5$) as the baseline network and tune these hyper-parameters. All these network variants are trained and tested on the DRIVE dataset with the same training configurations.

Table 3 and Fig. 5 show the influence of structural parameters in terms of AUC score. In Fig. 5, the point with $L = 0$ means the network structure with only mini-UNet, and the horizontal line represents the AUC score of a full-sized UNet. We can see that changing M or R only influences the performance slightly from the table. Instead, from the curve in Fig. 5, we can see that the AUC score increases with L , monotonically. It is reasonable to expect that the network performance would increase further more with larger L , because the IDNet is unfolded from the efficient optimization algorithm with convergence guarantee, for the convex image decomposition model. Note that less than 105 learnable parameters will be introduced by adding one ID layer. However, due to limited memory for the backpropagation, we conduct experiments with $L \leq 16$.

6.6. Comparisons with state-of-the-art neural networks. In this subsection, we take the IDmUNet ($M = 4, R = 2$ and $L = 16$). Table 2 shows the

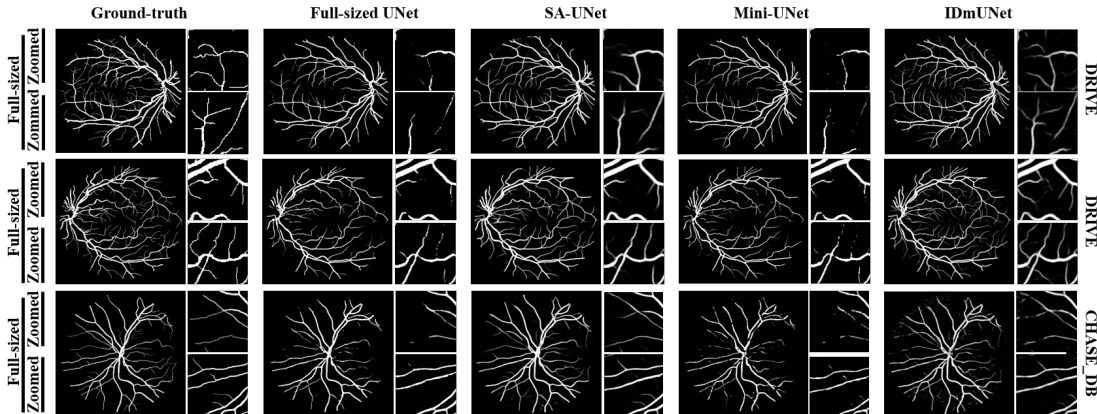


FIGURE 6. The ground-truth and segmentation results of full-sized UNet, SA-UNet, mini-UNet and IDmUNet. The first two rows are results from DRIVE dataset, whereas the last row is from CHASE-DB1. Each full-sized image is followed by two zoomed-in on its right side.

comparisons among the latest neural networks for retinal vessel segmentation and our IDmUNet on the most widely used DRIVE dataset. This table lists the shape of U-structure appeared in these networks, learnable parameters scale and the segmentation scores (AUC, ACC and MCC). Since we mainly focus on methods with a single U-structure, the shape partially shows the depth and width of networks. For the scale of learnable parameters, both the absolute value and the relative value are listed, with our IDmUNet as the baseline. Notice that some of them are provided by the literatures themselves and “-” means not available data. As one can see in Table 2, IDmUNet achieves the state-of-the-art results with far fewer learnable parameters. The AUC scores of SAUNet, AGNet, Vessel-Net, M2U-Net, UNet and IDmUNet are around a level of 0.9800 with a difference within 0.0100, but the parameter scale varies dramatically from 31.04m to 0.070m. The second smallest network in comparisons is SA-UNet [22], which is still 7 times larger than our IDmUNet. Additional results on CHASE_DB1 dataset are provided in Table 2.

Fig. 6 shows some visual results of the experiments. Our IDmUNet can recover more details, including small branches.

7. CONCLUSION

In this paper, we proposed a task-oriented network design for sparse feature segmentation. The sparsity prior on target objects can be clearly characterized by mathematical regularizer, while the complicated background needs trainable

architectures. So we started from a variational image decomposition model and derived an efficient scaled-ADMM solver for it. Following the idea of deep unfolding, IDNet, an image decomposition network, was constructed. Parameters in both the model and algorithm, as well as the part of regularization kernels, were relaxed to be learned. The IDNet was then combined with the mini-UNet, a shallow version of UNet, yielding the IDmUNet with applications to retinal vessel segmentation tasks.

IDmUNet effectively integrates the advantages of mathematical modeling and data-driven approaches. In experiments, our network achieved the state-of-the-art performance with far fewer learnable parameters, and behaved stable during the end-to-end training procedure. As the nature of deep unfolding methods, the median outputs of our IDNets (sub-nets of the IDmUNet) are still meaningful images, against the black-box behavior of many pure DNN methods. This property is quite valuable in practical use, especially for scenarios that require high confidence on results like medical image processing.

Our model-based and task-oriented network design strategy can be extended to other problems, where the mathematical modeling for targets are clear.

REFERENCES

- [1] Jonas Adler and Ozan Öktem. Learned Primal-Dual Reconstruction. *IEEE Transactions on Medical Imaging*, 37(6):1322–1332, 2018.
- [2] Jean-François Aujol, Guy Gilboa, Tony Chan, and Stanley Osher. Structure-Texture Image Decomposition—Modeling, Algorithms, and Parameter Selection. *International Journal of Computer Vision (IJCV)*, 67(1):111–136, April 2006.
- [3] Stephen Boyd. Distributed Optimization and Statistical Learning via the Alternating Direction Method of Multipliers. *FNT in Machine Learning*, 3(1):1–122, 2010.
- [4] Xiaohao Cai, Raymond Chan, Carola-Bibiane Schönlieb, Gabriele Steidl, and Tiejong Zeng. Linkage Between Piecewise Constant Mumford-Shah Model and ROF Model and Its Virtue in Image Segmentation. *SIAM Journal of Scientific Computing*, 41(6):B1310–B1340, 2019.
- [5] Xiaohao Cai, Raymond Chan, and Tiejong Zeng. A Two-Stage Image Segmentation Method Using a Convex Variant of the Mumford–Shah Model and Thresholding. *SIAM Journal on Imaging Sciences*, 6(1):368–390, January 2013.
- [6] Luca Calatroni, Juan Carlos De Los Reyes, and Carola-Bibiane Schönlieb. Infimal Convolution of Data Discrepancies for Mixed Noise Removal. *SIAM Journal on Imaging Sciences*, 10(3):1196–1233, January 2017.
- [7] E.J. Candes, J. Romberg, and T. Tao. Robust uncertainty principles: exact signal reconstruction from highly incomplete frequency information. *IEEE Transactions on Information Theory*, 52(2):489–509, 2006.
- [8] Antonin Chambolle and Pierre-Louis Lions. Image recovery via total variation minimization and related problems. *Numerische Mathematik*, 76(2):167–188, April 1997.
- [9] Huibin Chang, Weimin Huang, Chunlin Wu, Su Huang, Cuntai Guan, Sakthivel Sekar, Kishore Kumar Bhakoo, and Yuping Duan. A New Variational Method for Bias Correction and Its Applications to Rodent Brain Extraction. *IEEE Transactions on Medical Imaging*, 36(3):721–733, 2017.
- [10] Ricky T. Q. Chen, Yulia Rubanova, Jesse Bettencourt, and David K Duvenaud. Neural Ordinary Differential Equations. In S. Bengio, H. Wallach, H. Larochelle, K. Grauman,

- N. Cesa-Bianchi, and R. Garnett, editors, *Advances in Neural Information Processing Systems*, volume 31. Curran Associates, Inc., 2018.
- [11] Scott Shaobing Chen, David L. Donoho, and Michael A. Saunders. Atomic Decomposition by Basis Pursuit. *SIAM Journal on Scientific Computing*, 20(1):33–61, 1998.
- [12] D.L. Donoho. Compressed sensing. *IEEE Transactions on Information Theory*, 52(4):1289–1306, April 2006.
- [13] Yuping Duan, Huibin Chang, Weimin Huang, Jiayin Zhou, Zhongkang Lu, and Chunlin Wu. The L-0 Regularized Mumford-Shah Model for Bias Correction and Segmentation of Medical Images. *IEEE Transactions on Image Processing*, 24(11):3927–3938, November 2015.
- [14] Weinan E. A Proposal on Machine Learning via Dynamical Systems. *Communications in Mathematics and Statistics*, 5(1):1–11, 2017.
- [15] M.M. Fraz, P. Remagnino, A. Hoppe, B. Uyyanonvara, A.R. Rudnicka, C.G. Owen, and S.A. Barman. Blood vessel segmentation methodologies in retinal images – A survey. *Computer Methods and Programs in Biomedicine*, 108(1):407–433, October 2012.
- [16] Muhammad Moazam Fraz, Paolo Remagnino, Andreas Hoppe, Bunyarit Uyyanonvara, Alicja R. Rudnicka, Christopher G. Owen, and Sarah A. Barman. An Ensemble Classification-Based Approach Applied to Retinal Blood Vessel Segmentation. *IEEE Transactions on Biomedical Engineering*, 59(9):2538–2548, September 2012.
- [17] Samy Wu Fung, Howard Heaton, Qiuwei Li, Daniel McKenzie, Stanley Osher, and Wotao Yin. JFB: Jacobian-Free Backpropagation for Implicit Networks. *arXiv:2103.12803 [cs]*, September 2021.
- [18] Roland Glowinski and Americo Marroco. Sur l’approximation, par éléments finis d’ordre un, et la résolution, par pénalisation-dualité d’une classe de problèmes de Dirichlet non linéaires. *ESAIM: Mathematical Modelling and Numerical Analysis-Modélisation Mathématique et Analyse Numérique*, 9(R2):41–76, 1975.
- [19] Roland Glowinski, Stanley J Osher, and Wotao Yin. *Splitting methods in communication, imaging, science, and engineering*. Springer, 2017.
- [20] Karol Gregor and Yann LeCun. Learning Fast Approximations of Sparse Coding. In *Proceedings of the 27th International Conference on International Conference on Machine Learning, ICML’10*, pages 399–406. Omnipress, 2010.
- [21] Zaiwang Gu, Jun Cheng, Huazhu Fu, Kang Zhou, Huaying Hao, Yitian Zhao, Tianyang Zhang, Shenghua Gao, and Jiang Liu. CE-Net: Context Encoder Network for 2D Medical Image Segmentation. *IEEE Transactions on Medical Imaging*, 38(10):2281–2292, October 2019.
- [22] Changlu Guo, Márton Szemenyei, Yugen Yi, Wenle Wang, Buer Chen, and Changqi Fan. SA-UNet: Spatial Attention U-Net for Retinal Vessel Segmentation. In *2020 25th International Conference on Pattern Recognition (ICPR)*, pages 1236–1242, January 2021.
- [23] Xueyan Guo, Yunhua Xue, and Chunlin Wu. Effective Two-Stage Image Segmentation: A New Non-Lipschitz Decomposition Approach with Convergent Algorithm. *J Math Imaging Vis*, 63(3):356–379, March 2021.
- [24] Bumsu Ham, Minsu Cho, and Jean Ponce. Robust Guided Image Filtering Using Nonconvex Potentials. *IEEE Transactions on Pattern Analysis and Machine Intelligence*, 40(1):192–207, January 2018.
- [25] Kelei He, Chunfeng Lian, Bing Zhang, Xin Zhang, Xiaohuan Cao, Dong Nie, Yang Gao, Junfeng Zhang, and Dinggang Shen. HF-UNet: Learning Hierarchically Inter-Task Relevance in Multi-Task U-Net for Accurate Prostate Segmentation in CT Images. *IEEE Transactions on Medical Imaging*, 40(8):2118–2128, 2021.
- [26] Howard Heaton, Samy Wu Fung, Aviv Gibali, and Wotao Yin. Feasibility-based Fixed Point Networks. *arXiv:2104.14090 [cs]*, April 2021.

- [27] John R. Hershey, Jonathan Le Roux, and Felix Weninger. Deep Unfolding: Model-Based Inspiration of Novel Deep Architectures. *arXiv:1409.2574 [cs, stat]*, November 2014.
- [28] Huimin Huang, Lanfen Lin, Ruofeng Tong, Hongjie Hu, Qiaowei Zhang, Yutaro Iwamoto, Xianhua Han, Yen-Wei Chen, and Jian Wu. UNet 3+: A Full-Scale Connected UNet for Medical Image Segmentation. In *ICASSP 2020 - 2020 IEEE International Conference on Acoustics, Speech and Signal Processing (ICASSP)*, pages 1055–1059, 2020.
- [29] Miyoung Jung and Myungjoo Kang. Simultaneous Cartoon and Texture Image Restoration with Higher-Order Regularization. *SIAM Journal on Imaging Sciences*, 8(1):721–756, January 2015.
- [30] Sharif Amit Kamran, Khondker Fariha Hossain, Alireza Tavakkoli, Stewart Lee Zuckerbrod, Kenton M Sanders, and Salah A Baker. RV-GAN: Segmenting Retinal Vascular Structure in Fundus Photographs Using a Novel Multi-scale Generative Adversarial Network. In *International Conference on Medical Image Computing and Computer-Assisted Intervention*, pages 34–44. Springer, 2021.
- [31] Li-Wei Kang, Chia-Wen Lin, and Yu-Hsiang Fu. Automatic single-image-based rain streaks removal via image decomposition. *IEEE Transactions on Image Processing*, 21(4):1742–1755, 2011.
- [32] Youngjung Kim, Bumsub Ham, Minh N. Do, and Kwanghoon Sohn. Structure-Texture Image Decomposition Using Deep Variational Priors. *IEEE Transactions on Image Processing*, 28(6):2692–2704, June 2019.
- [33] Ron Kimmel, Michael Elad, Doron Shaked, Renato Keshet, and Irwin Sobel. A variational framework for retinex. *International Journal of computer vision*, 52(1):7–23, 2003.
- [34] Tim Laibacher, Tillman Weyde, and Sepehr Jalali. M2U-Net: Effective and Efficient Retinal Vessel Segmentation for Real-World Applications. In *2019 IEEE/CVF Conference on Computer Vision and Pattern Recognition Workshops (CVPRW)*, pages 115–124. IEEE, June 2019.
- [35] Edwin H. Land and John J. McCann. Lightness and Retinex Theory. *Journal of the Optical Society of America*, 61(1):1, January 1971.
- [36] Huaifeng Li, Xiaoge He, Dapeng Tao, Yuanyan Tang, and Ruxin Wang. Joint medical image fusion, denoising and enhancement via discriminative low-rank sparse dictionaries learning. *Pattern Recognition*, 79:130–146, July 2018.
- [37] Liangzhi Li, Manisha Verma, Yuta Nakashima, Hajime Nagahara, and Ryo Kawasaki. Iter-Net: Retinal Image Segmentation Utilizing Structural Redundancy in Vessel Networks. In *2020 IEEE Winter Conference on Applications of Computer Vision (WACV)*, pages 3645–3654, 2020.
- [38] Jingwei Liang and Xiaoqun Zhang. Retinex by Higher Order Total Variation \mathbb{L}^1 Decomposition. *Journal of Mathematical Imaging and Vision*, 52(3):345–355, 2015.
- [39] Zichao Long, Yiping Lu, and Bin Dong. PDE-Net 2.0: Learning PDEs from Data with A Numeric-Symbolic Hybrid Deep Network. *Journal of Computational Physics*, 399:108925, December 2019. arXiv: 1812.04426 version: 2.
- [40] Zichao Long, Yiping Lu, Xianzhong Ma, and Bin Dong. Pde-net: Learning pdes from data. In *International Conference on Machine Learning*, pages 3208–3216. PMLR, 2018.
- [41] Wenye Ma, Stanley Osher, and Department of Mathematics, UCLA, Los Angeles, CA 90095-1555. A TV Bregman iterative model of Retinex theory. *Inverse Problems & Imaging*, 6(4):697–708, 2012.
- [42] Michael K. Ng and Wei Wang. A Total Variation Model for Retinex. *SIAM Journal on Imaging Sciences*, 4(1):345–365, January 2011.

- [43] Olaf Ronneberger, Philipp Fischer, and Thomas Brox. U-Net: Convolutional Networks for Biomedical Image Segmentation. In *Medical Image Computing and Computer-Assisted Intervention*, pages 234–241. Springer, 2015.
- [44] Hayden Schaeffer and Stanley Osher. A low patch-rank interpretation of texture. *SIAM Journal on Imaging Sciences*, 6(1):226–262, 2013.
- [45] Uwe Schmidt and Stefan Roth. Shrinkage Fields for Effective Image Restoration. In *2014 IEEE Conference on Computer Vision and Pattern Recognition*, pages 2774–2781. IEEE, June 2014.
- [46] S. Setzer, G. Steidl, and T. Teuber. Infimal convolution regularization with discrete $l(1)$ -type functionals. *Communications in mathematical sciences*, 9(3):797–827, September 2011.
- [47] J. Staal, M.D. Abramoff, M. Niemeijer, M.A. Viergever, and B. van Ginneken. Ridge-Based Vessel Segmentation in Color Images of the Retina. *IEEE Transactions on Medical Imaging*, 23(4):501–509, April 2004.
- [48] Jian Sun and Marshall F. Tappen. Learning non-local range Markov Random field for image restoration. In *CVPR 2011*, pages 2745–2752, 2011.
- [49] Bo Wang, Shuang Qiu, and Huiguang He. Dual encoding u-net for retinal vessel segmentation. In *International Conference on Medical Image Computing and Computer-Assisted Intervention*, pages 84–92. Springer, 2019.
- [50] Yilun Wang, Junfeng Yang, Wotao Yin, and Yin Zhang. A New Alternating Minimization Algorithm for Total Variation Image Reconstruction. *SIAM Journal on Imaging Sciences*, 1(3):248–272, January 2008.
- [51] Ezra Winston and J Zico Kolter. Monotone operator equilibrium networks. *Advances in Neural Information Processing Systems*, 33:10718–10728, 2020.
- [52] Chunlin Wu and Xue-Cheng Tai. Augmented Lagrangian Method, Dual Methods, and Split Bregman Iteration for ROF, Vectorial TV, and High Order Models. *SIAM Journal on Imaging Sciences*, 3(3):300–339, January 2010.
- [53] Yicheng Wu, Yong Xia, Yang Song, Donghao Zhang, Dongnan Liu, Chaoyi Zhang, and Weidong Cai. Vessel-Net: Retinal Vessel Segmentation Under Multi-path Supervision. In *Medical Image Computing and Computer Assisted Intervention*, volume 11764, pages 264–272. Springer, 2019.
- [54] Yicheng Wu, Yong Xia, Yang Song, Yanning Zhang, and Weidong Cai. Multiscale Network Followed Network Model for Retinal Vessel Segmentation. In *Medical Image Computing and Computer Assisted Intervention*, volume 11071, pages 119–126. Springer, 2018.
- [55] Jun Xu, Yingkun Hou, Dongwei Ren, Li Liu, Fan Zhu, Mengyang Yu, Haoqian Wang, and Ling Shao. STAR: A Structure and Texture Aware Retinex Model. *IEEE Transactions on Image Processing*, 29:5022–5037, 2020.
- [56] Yan Yang, Jian Sun, Huibin Li, and Zongben Xu. Deep ADMM-Net for Compressive Sensing MRI. In *Proceedings of the 30th International Conference on Neural Information Processing Systems*, NIPS’16, pages 10–18. Curran Associates Inc., 2016.
- [57] Yan Yang, Jian Sun, Huibin Li, and Zongben Xu. ADMM-CSNet: A Deep Learning Approach for Image Compressive Sensing. *IEEE Transactions on Pattern Analysis and Machine Intelligence*, 42(3):521–538, March 2020.
- [58] Fisher Yu and Vladlen Koltun. Multi-scale context aggregation by dilated convolutions. In *International Conference on Learning Representations*, 2016.
- [59] Shihao Zhang, Huazhu Fu, Yuguang Yan, Yubing Zhang, Qingyao Wu, Ming Yang, Mingkui Tan, and Yanwu Xu. Attention Guided Network for Retinal Image Segmentation. *arXiv:1907.12930 [cs, eess]*, October 2019.

- [60] Hengshuang Zhao, Jianping Shi, Xiaojuan Qi, Xiaogang Wang, and Jiaya Jia. Pyramid scene parsing network. In *Proceedings of the IEEE conference on computer vision and pattern recognition*, pages 2881–2890, 2017.
- [61] Yuqian Zhou, Hanchao Yu, and Humphrey Shi. Study Group Learning: Improving Retinal Vessel Segmentation Trained with Noisy Labels. In *Medical Image Computing and Computer Assisted Intervention*, pages 57–67. Springer, 2021.
- [62] Zongwei Zhou, Md Mahfuzur Rahman Siddiquee, Nima Tajbakhsh, and Jianming Liang. UNet++: Redesigning Skip Connections to Exploit Multiscale Features in Image Segmentation. *IEEE Transactions on Medical Imaging*, 39(6):1856–1867, June 2020.